Chapter 2
Low Frequency Dynamic Model

Like other converters in the switched mode power converter family, operation of matrix converters involves two significant frequency components. These are the fundamental frequency and the switching frequency. The fundamental frequency component is associated with power transfer while the switching component is a byproduct of the operation. If these switching components are injected into the grid side or to the load side it would lead to undesirable consequences and thus it is necessary to filter them. The filtering process has been discussed in detail in a later chapter. For this chapter, it is sufficient to have the understanding that low pass filters are realized by passive elements in these converters. For a given power level, the size of these filter components reduces as the switching frequency becomes higher. Hence a large difference between the switching frequency and the fundamental component is always preferable as it helps to achieve effective filtering with smaller components size. The switching frequencies are in the order kHzs, or tens of kHzs, a number which depends upon the rated power handling capacity of the converter. On the other hand, the order of the fundamental component is usually tens of Hertz. For any well designed converter, the switching frequency component in the output variables are negligible compared to the fundamental frequency component. Therefore, while deriving a model which represents the dynamic behaviour of the converter the high switching frequency component can be neglected without any loss of accuracy in modelling. Thus the control scheme of MC or for many other SMPCs has to be devised such that the fundamental frequency component and low frequency harmonic components can be processed with a desired degree of accuracy.

This chapter presents an analysis of the linearized low frequency model of MC, where it has been used as a 3-phase regulated sinusoidal voltage supply. The objectives of all modulation techniques for MC are attaining the desired—amplitude, phase and frequency of the output voltages and IDF at the input side. In the first section of this chapter, the modulation technique adopted in this work is briefly discussed to describe the low frequency gain of MC. It has been subsequently used to develop the linearized dynamic model in Sect. 2.2 from where the plant transfer function matrix

A. Dasgupta and P. Sensarma, *Design and Control of Matrix Converters*,
Energy Systems in Electrical Engineering, DOI 10.1007/978-981-10-3831-0_2

is derived. In Sect. 2.3 it is demonstrated how the system poles/zeros are affected by input voltage, input displacement factor, throughput power and parameters of the input filter. In the process it is found that based on the operating points, right half zeros may emerge in the control to output transfer functions beyond a critical level of input power.

2.1 Low Frequency Gain of 3-Phase MC

The phase to input side neutral voltages applied to the converter i.e. the voltages at terminals a, b and c with reference to the input neutral shown in Fig. 2.1 are represented as

$$\begin{bmatrix} v_a \\ v_b \\ v_c \end{bmatrix} = \mathbf{v_{cf}}^{(3)} = \hat{V}_{cf} \begin{bmatrix} \cos(\omega_i t - \varphi_c) \\ \cos(\omega_i t - \varphi_c - 120°) \\ \cos(\omega_i t - \varphi_c + 120°) \end{bmatrix}. \tag{2.1}$$

These voltages appear across the input filter capacitor C_f depicted in the per-phase diagram shown in Fig. 1.9b and reproduced in Fig. 2.2. MC allows control on the magnitude, frequency and phase of the output voltage and IDF. Let the desired output voltages, referred to output neutral n, be described as

$$\mathbf{v^*_{on}}^{(3)} = \begin{bmatrix} v^*_{An} \\ v^*_{Bn} \\ v^*_{Cn} \end{bmatrix} = \hat{V}_o \begin{bmatrix} \cos(\omega_o t + \varphi_o) \\ \cos(\omega_o t + \varphi_o - 120°) \\ \cos(\omega_o t + \varphi_o + 120°) \end{bmatrix}, \tag{2.2}$$

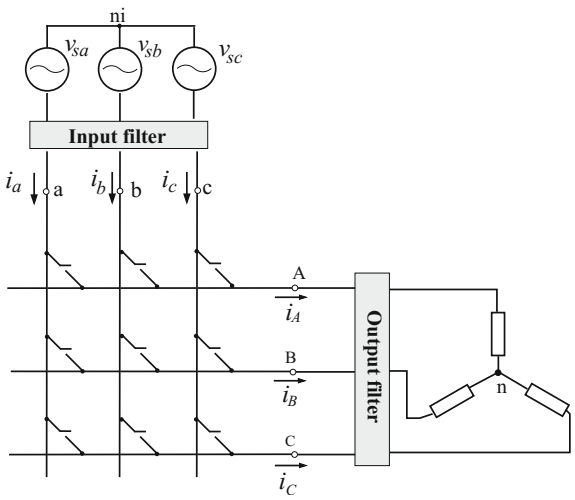

Fig. 2.1 Schematic of a 3-ph MC

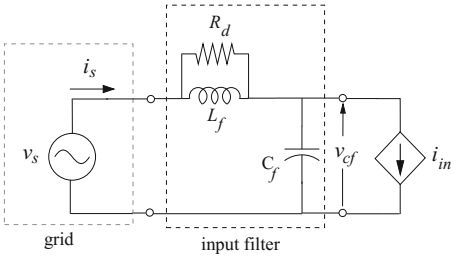

Fig. 2.2 Input side equivalent circuit for the per-phase system

where * indicates reference signal. The corresponding line to line voltages are

$$\mathbf{v^*_{oL}}^{(3)} = \begin{bmatrix} v^*_{An} - v^*_{Bn} \\ v^*_{Bn} - v^*_{Cn} \\ v^*_{Cn} - v^*_{An} \end{bmatrix} = \begin{bmatrix} v^*_{AB} \\ v^*_{BC} \\ v^*_{CA} \end{bmatrix} = \sqrt{3}\hat{V}_o \begin{bmatrix} \cos(\omega_o t + \varphi_o + 30°) \\ \cos(\omega_o t + \varphi_o + 30° - 120°) \\ \cos(\omega_o t + \varphi_o + 30° + 120°) \end{bmatrix}. \tag{2.3}$$

Indirect space vector modulation (ISVM) [25] method has been adopted in this work to synthesize the desired voltage output. The basic principle of this method is discussed in the following section.

2.1.1 *Indirect Space Vector Modulation (ISVM) Approach*

In ISVM technique the 9 bidirectional switch MC structure is conceptually decoupled into an equivalent cascaded chain of fictitious current and voltage source converters (CSC and VSC) as shown in Fig. 2.3. The imaginary DC link voltage and current i.e. V_{dc} and I_{dc} are treated as sources for the VSC and CSC parts respectively. The duty cycle of each switch in the 9 bidirectional switch MC structure is calculated in two stages. In the first stage, the duty cycles are calculated separately for each converters of the decoupled construct using conventional space vector modulation (SVM)

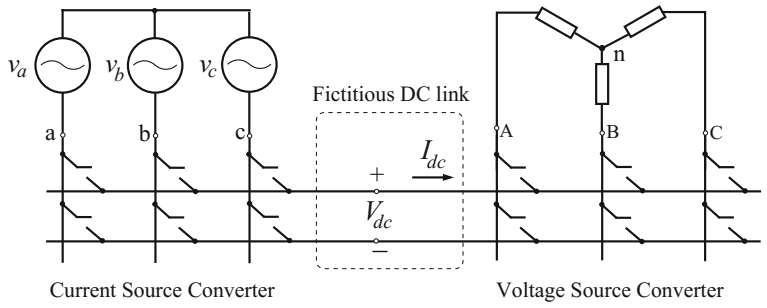

Fig. 2.3 Decoupled current and voltage source converter construct

approach. In the next stage, the individual duty cycles are combined based on instantaneous active power balance between the input and output sides. The duty cycle of the 12 switch fictitious CSC–VSC structure can be then directly mapped to the 9 bidirectional switch MC topology.

To illustrate this procedure, the VSC part is considered first, where the reference line to line voltages are used to define the vector

$$\bar{\mathbf{V}}^{*}_{\mathbf{oL}} = \sqrt{\frac{2}{3}}\left(v^{*}_{AB} + v^{*}_{BC}\, e^{j2\pi/3} + v^{*}_{CA}\, e^{-j2\pi/3}\right). \tag{2.4}$$

Here the constant multiplier $\sqrt{2/3}$ ensures power invariant transformations. Substituting the line voltages from (2.3) in (2.4), $\bar{\mathbf{V}}^{*}_{\mathbf{oL}}$ is obtained as

$$\bar{\mathbf{V}}^{*}_{\mathbf{oL}} = \frac{3}{\sqrt{2}}\,\hat{V}_o\, e^{j(\omega_o t+\varphi_o+30^\circ)}. \tag{2.5}$$

Referring to Fig. 2.3, there are 8 valid switching combinations by which the output terminals of the VSC can be connected to the fictitious DC link. Here, the term valid combinations refers to those which ensure that any output terminal is never left open. The line voltages corresponding to each of these combinations are used to create the vector

$$\bar{\mathbf{V}}_{\mathbf{oL}} = \sqrt{\frac{2}{3}}\left(v_{AB} + v_{BC}\, e^{j2\pi/3} + v_{CA}\, e^{-j2\pi/3}\right). \tag{2.6}$$

Applying (2.6) to each of the 8 combinations result in stationary vectors (SV) which are sometimes also referred to as switching state vectors. These are tabulated in Table 2.1 and also shown in Fig. 2.4a.

Table 2.1 Switching state vectors for the VSC

A	B	C	$\bar{\mathbf{V}}_{\mathbf{oL}}$	Stationary vectors
+	–	–	$\sqrt{\frac{2}{3}}\,[V_{dc} + 0 - V_{dc}\, e^{-j2\pi/3}] = \sqrt{2}V_{dc}\angle 30^\circ$	$\mathbf{V}_1$
+	+	–	$\sqrt{\frac{2}{3}}\,[0 + V_{dc}\, e^{j2\pi/3} - V_{dc}\, e^{-j2\pi/3}] = \sqrt{2}V_{dc}\angle 90^\circ$	$\mathbf{V}_2$
–	+	–	$\sqrt{\frac{2}{3}}\,[-V_{dc} + V_{dc}\, e^{j2\pi/3} + 0] = \sqrt{2}V_{dc}\angle 150^\circ$	$\mathbf{V}_3$
–	+	+	$\sqrt{\frac{2}{3}}\,[-V_{dc} + 0 + V_{dc}\, e^{-j2\pi/3}] = \sqrt{2}V_{dc}\angle 210^\circ$	$\mathbf{V}_4$
–	–	+	$\sqrt{\frac{2}{3}}\,[0 + -V_{pn}\, e^{j2\pi/3} + V_{pn}\, e^{-j2\pi/3}] = \sqrt{2}V_{dc}\angle 270^\circ$	$\mathbf{V}_5$
+	–	+	$\sqrt{\frac{2}{3}}\,[V_{pn} - V_{pn}\, e^{j2\pi/3} + 0] = \sqrt{2}V_{dc}\angle 330^\circ$	$\mathbf{V}_6$
–	–	–	$\sqrt{\frac{2}{3}}\,[0 + 0 + 0] = 0$	$\mathbf{V}_0$
+	+	+		

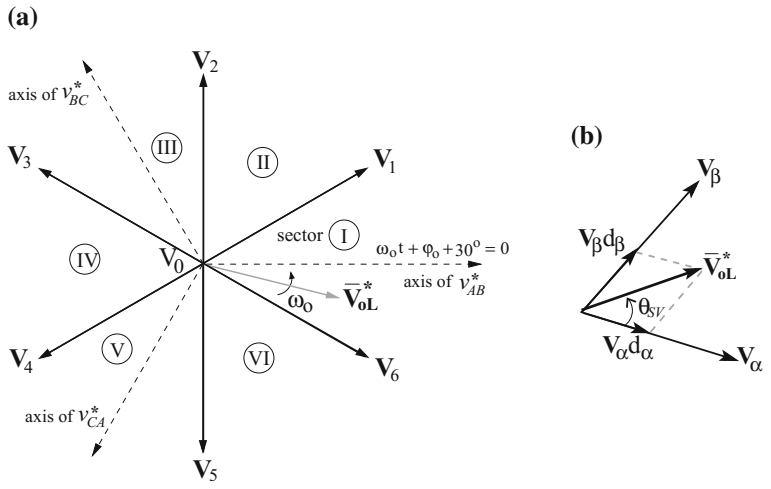

Fig. 2.4 **a** Output voltage stationary vectors and $\bar{\mathbf{V}}^*_{\mathbf{oL}}$. **b** Synthesizing $\bar{\mathbf{V}}^*_{\mathbf{oL}}$

It is evident that there are 6 sets of SVs with non zero magnitude having distinct spatial orientation and 2 sets of SVs with zero magnitude. The objective of SVM is to synthesize $\bar{\mathbf{V}}^*_{\mathbf{oL}}$, in a time-averaged sense, over a switching period (T_S), by using the available SVs as

$$\int_0^{T_S} \bar{\mathbf{V}}^*_{\mathbf{oL}} dt = \int_0^{T_S} \bar{\mathbf{V}}_{\mathbf{oL}} dt. \tag{2.7}$$

Since the switching frequency (f_S) is much higher than the fundamental frequency, $\bar{\mathbf{V}}^*_{\mathbf{oL}}$ practically behaves like a stationary vector over a single switching period. So with appropriate scaling, many combinations of SVs can be used to synthesize the target voltage vector $\bar{\mathbf{V}}^*_{\mathbf{oL}}$. However, using two adjacent SVs leads to minimum number of switching. Additionally, the instantaneous voltage deviation $\bar{\mathbf{V}}^*_{\mathbf{oL}} - \bar{\mathbf{V}}_{\mathbf{oL}}$ is lowest, which ensures minimum current ripple in the inductors connected to the output terminals. The adjacent SVs, $\mathbf{V}_\alpha$ and $\mathbf{V}_\beta$, are shown in Fig. 2.4b trailing and leading $\bar{\mathbf{V}}^*_{\mathbf{oL}}$ respectively. θ_{SV} is the instantaneous angle between $\bar{\mathbf{V}}^*_{\mathbf{oL}}$ and $\mathbf{V}_\alpha$. Over a single switching period T_S, assumption of a stationary $\bar{\mathbf{V}}^*_{\mathbf{oL}}$ implies a constant θ_{SV}. Therefore, $\bar{\mathbf{V}}^*_{\mathbf{oL}}$ can be synthesized as

$$\begin{aligned} \bar{\mathbf{V}}^*_{\mathbf{oL}} &= \mathbf{V}_\alpha \frac{T_\alpha}{T_S} + \mathbf{V}_\beta \frac{T_\beta}{T_S} \\ &= \mathbf{V}_\alpha d_\alpha + \mathbf{V}_\beta d_\beta. \end{aligned} \tag{2.8}$$

Applying properties of triangle,

$$\frac{|\bar{\mathbf{V}}^*_{\mathbf{oL}}|}{\sin 120^\circ} = \frac{|\mathbf{V}_\alpha d_\alpha|}{\sin(60^\circ - \theta_{SV})} = \frac{|\mathbf{V}_\beta d_\beta|}{\sin(\theta_{SV})}. \tag{2.9}$$

Table 2.2 Line voltages, when $\bar{\mathbf{V}}^*_{\mathbf{oL}}$ is in sector I

	ON time	A	B	C		v_{AB}	v_{BC}	v_{CA}
During d_6 (d_α)	$d_\alpha T_S$	+	−	+	$\longrightarrow$	V_{dc}	$-V_{dc}$	0
During d_1 (d_β)	$d_\beta T_S$	+	−	−	$\longrightarrow$	V_{dc}	0	$-V_{dc}$

Using (2.5), Table 2.1 and (2.9), d_α and d_β are determined as

$$d_\alpha = \frac{\sqrt{3}\,\hat{V}_o}{V_{dc}} \sin(60^\circ - \theta_{SV}) = m_v \sin(60^\circ - \theta_{SV}),$$
$$d_\beta = \frac{\sqrt{3}\,\hat{V}_o}{V_{dc}} \sin(\theta_{SV}) = m_v \sin(\theta_{SV}). \tag{2.10}$$

As an example, let $\bar{\mathbf{V}}^*_{\mathbf{oL}}$ be considered to be lying in sector I. Here $\mathbf{V}_\alpha = \mathbf{V}_6$ and $\mathbf{V}_\beta = \mathbf{V}_1$. Using Table 2.1, the line voltages corresponding to the two duty cycles are shown in Table 2.2.

Using (2.10) and Table 2.2, the average value of the synthesized output voltages over T_S, when $\bar{\mathbf{V}}_{\mathbf{oL}}$ is in sector I, are obtained as

$$\mathbf{v_{oL}}^{(3)} = \begin{bmatrix} v_{AB} \\ v_{BC} \\ v_{CA} \end{bmatrix} = \begin{bmatrix} d_\alpha + d_\beta \\ -d_\alpha \\ -d_\beta \end{bmatrix} V_{dc} = m_v \begin{bmatrix} \cos(\theta_{SV} - 30^\circ) \\ -\sin(60^\circ - \theta_{SV}) \\ -\sin(\theta_{SV}) \end{bmatrix} V_{dc}. \tag{2.11}$$

Again from Fig. 2.4a, b, when $\bar{\mathbf{V}}_{\mathbf{oL}}$ is in sector I, θ_{SV} can be evaluated in terms of output voltage frequency and phase as

$$\theta_{SV} - (\omega_o t + \varphi_0 + 30^\circ) = 30^\circ \implies \theta_{SV} = \omega_o t + \varphi_o + 60^\circ. \tag{2.12}$$

Substituting θ_{SV} from (2.12) in (2.11), the output voltages can be expressed as

$$\mathbf{v_{oL}}^{(3)} = \underbrace{m_v \begin{bmatrix} \cos(\omega_o t + \varphi_o + 30^\circ) \\ \cos(\omega_o t + \varphi_o + 30^\circ - 120^\circ) \\ \cos(\omega_o t + \varphi_o + 30^\circ + 120^\circ) \end{bmatrix}}_{\mathbf{m_v}} V_{dc} = \mathbf{m_v} V_{dc}, \tag{2.13}$$

where $\mathbf{m_v}$ represents the low frequency gain matrix of the VSC part.

Using Table 2.1, Fig. 2.4a, b, the ratio of the output voltages to V_{dc} and θ_{SV} in terms of output voltage frequency and phase for sectors II to VI are tabulated in Table 2.3. For all the sectors, evaluation of the average value of the synthesized output voltages results in the expression described by (2.13).

Table 2.3 Ratio of line voltages to V_{dc}, θ_{SV} for sectors II to VI

	v_{AB}/V_{dc}	v_{BC}/V_{dc}	v_{CA}/V_{dc}	θ_{SV}
Sector II	d_α	d_β	$-d_\alpha - d_\beta$	$\omega_o t + \varphi_0$
Sector III	$-d_\beta$	$d_\alpha + d_\beta$	$-d_\alpha$	$\omega_o t + \varphi_0 - 60°$
Sector IV	$-d_\alpha - d_\beta$	d_α	d_β	$\omega_o t + \varphi_0 - 120°$
Sector V	$-d_\alpha$	$-d_\beta$	$d_\alpha + d_\beta$	$\omega_o t + \varphi_0 - 180°$
Sector VI	d_β	$-d_\alpha - d_\beta$	d_α	$\omega_o t + \varphi_0 - 240°$

Table 2.4 Switching state vectors for CSC

+	–	$\bar{\mathbf{I}}_{\mathbf{in}}$	State vectors
a	c	$\sqrt{2}I_{dc}\angle 30°$	$\mathbf{I}_1$
b	c	$\sqrt{2}I_{dc}\angle 90°$	$\mathbf{I}_2$
b	a	$\sqrt{2}I_{dc}\angle 150°$	$\mathbf{I}_3$
c	a	$\sqrt{2}I_{dc}\angle 210°$	$\mathbf{I}_4$
c	b	$\sqrt{2}I_{dc}\angle 270°$	$\mathbf{I}_5$
a	b	$\sqrt{2}I_{dc}\angle 330°$	$\mathbf{I}_6$
a	a	0	I_0
b	b		
c	c		

The low frequency gain matrix of the CSC part is derived in a similar manner. If φ_i is the desired input displacement angle, the desired input currents are then represented as

$$\mathbf{i}_{\mathbf{in}}^{*\,(3)} = \begin{bmatrix} i_a^* \\ i_b^* \\ i_c^* \end{bmatrix} = \hat{I}_{in} \begin{bmatrix} \cos(\omega_i t - \varphi_c - \varphi_i) \\ \cos(\omega_i t - \varphi_c - \varphi_i - 120°) \\ \cos(\omega_i t - \varphi_c - \varphi_i + 120°) \end{bmatrix}, \tag{2.14}$$

and therefore the target input current rotating vector is

$$\bar{\mathbf{I}}_{\mathbf{in}}^* = \sqrt{\frac{2}{3}}\,(i_a^* + i_b^*\, e^{j2\pi/3} + i_c^*\, e^{-j2\pi/3}) = \sqrt{\frac{3}{2}}\hat{I}_{in}\, e^{j(\omega_i t - \varphi_c - \varphi_i)}. \tag{2.15}$$

The valid switching states along with the SVs are tabulated in Table 2.4. Figure 2.5 shows the SVs of the CSC construct.

The duty cycles for the switches of the fictitious CSC part are determined in the same manner as their VSC counterparts. They are

$$d_\mu = \frac{\hat{I}_{in}}{I_{dc}} \sin(60° - \theta_{SI}) = m_i \sin(60° - \theta_{SI}) \quad \& \quad d_\gamma = \frac{\hat{I}_{in}}{I_{dc}} \sin(\theta_{SI}) = m_i \sin(\theta_{SI}). \tag{2.16}$$

Table 2.5 Input currents when $\bar{\mathbf{I}}_{\mathbf{in}}^{*}$ is in sector I

	+	−		i_a	i_b	i_c
During d_6 (d_μ)	a	b	$\longrightarrow$	I_{dc}	$-I_{dc}$	0
During d_1 (d_γ)	a	c	$\longrightarrow$	I_{dc}	0	$-I_{dc}$

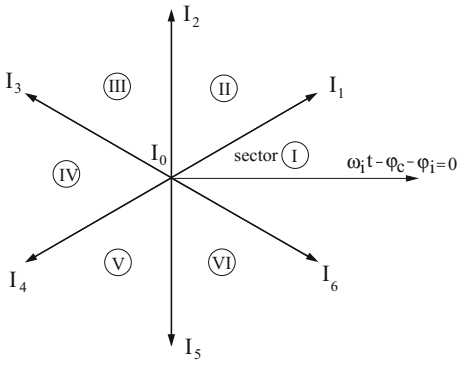

Fig. 2.5 Input current vectors

Here, θ_{SI}, μ, γ are analogous to $\theta_{SV}, \alpha, \beta$ in Fig. 2.4b. When $\bar{\mathbf{I}}_{\mathbf{in}}^{*}$ is in sector I, where $\mathbf{I}_\mu = \mathbf{I}_6$ and $\mathbf{I}_\gamma = \mathbf{I}_1$, the input currents are shown in Table 2.5.

Additionally, for sector I, θ_{SI} can be expressed as

$$\theta_{SI} = \omega_i t - \varphi_c - \varphi_i + 30^\circ. \tag{2.17}$$

Using (2.16), (2.17) and Table 2.5, the synthesized input phase currents are

$$\mathbf{i_{in}}^{(3)} = \begin{bmatrix} i_a \\ i_b \\ i_c \end{bmatrix} = \begin{bmatrix} d_\mu + d_\gamma \\ -d_\mu \\ -d_\gamma \end{bmatrix} I_{dc} = \underbrace{m_i \begin{bmatrix} \cos(\omega_i t - \varphi_c - \varphi_i) \\ \cos(\omega_i t - \varphi_c - \varphi_i - 120^\circ) \\ \cos(\omega_i t - \varphi_c - \varphi_i + 120^\circ) \end{bmatrix}}_{\mathbf{m_i}} I_{dc}$$
$$= \mathbf{m_i} I_{dc}, \tag{2.18}$$

where $\mathbf{m_i}$ represents the low frequency gain matrix of the CSC part. The ratio of the input current to I_{dc} and θ_{SI} in terms of input current frequency and phase for sectors II–VI are tabulated in Table 2.6.

From the discussion based on separate CSC and VSC structure, it seems that both $\mathbf{v}_{\mathbf{oL}}^{*}{}^{(3)}$ and $\mathbf{i}_{\mathbf{in}}^{*}{}^{(3)}$ can be synthesized independently. This would imply that the duration of active vectors in one converter, i.e. those corresponding to active power flow, can be independent of the active power flow duration in the second converter. However this is not possible. As an example, a zero vector for VSC means all 3 output phases are connected to the same DC link terminal—resulting in zero I_{dc}. Hence, a nonzero

Table 2.6 Ratio of input currents to I_{dc}, θ_{SI} for sectors II–VI

	i_a/I_{dc}	i_b/I_{dc}	i_c/I_{dc}	θ_{SI}
Sector II	d_μ	d_γ	$-d_\mu - d_\gamma$	$\omega_i t - \varphi_c - \varphi_i - 30°$
Sector III	$-d_\gamma$	$d_\mu + d_\gamma$	$-d_\mu$	$\omega_i t - \varphi_c - \varphi_i - 90°$
Sector IV	$-d_\mu - d_\gamma$	d_μ	d_γ	$\omega_i t - \varphi_c - \varphi_i - 150°$
Sector V	$-d_\mu$	$-d_\gamma$	$d_\mu + d_\gamma$	$\omega_i t - \varphi_c - \varphi_i - 210°$
Sector VI	d_γ	$-d_\mu - d_\gamma$	d_μ	$\omega_i t - \varphi_c - \varphi_i - 270°$

$\bar{\mathbf{I}}_{\mathbf{in}}^{*}$ cannot be synthesized during this period. Therefore, at a given instant of time, it is not possible to have an active vector in one converter and a zero vector in the other one. This is where the second stage of duty cycle computation begins as described in the following.

Absence of any intermediate storage element in the power stage of MC implies that instantaneous active power at the input and output side must be same. This power balance necessarily requires that the active vector states of VSC and CSC must be chosen at the same instant and applied for exactly the same duration. This requires combining the gain matrices of the VSC and CSC parts. If P_{in} be the throughput power, then using (2.18),

$$P_{in} = \{\mathbf{i_{in}}^{(3)}\}^T \mathbf{v_{cf}}^{(3)} = \{\mathbf{m_i}\}^T I_{dc} \mathbf{v_{cf}}^{(3)} = \{\mathbf{m_i}\}^T \frac{P_{in}}{V_{dc}} \mathbf{v_{cf}}^{(3)} \implies V_{dc} = \{\mathbf{m_i}\}^T \mathbf{v_{cf}}^{(3)}. \tag{2.19}$$

Subsequently, substituting V_{dc} in (2.13) by using (2.19), the voltage gain relation is obtained as

$$\mathbf{v_{oL}}^{(3)} = \mathbf{m_v}\{\mathbf{m_i}\}^T \mathbf{v_{cf}}^{(3)}. \tag{2.20}$$

Hence $\mathbf{m_v}\{\mathbf{m_i}\}^T$ is the input phase to output line voltage low frequency gain matrix. Using (2.13) and (2.18), this gain is evaluated as

$$\mathbf{m_v}\{\mathbf{m_i}\}^T = \underbrace{m_v m_i}_{m} \begin{bmatrix} \cos(\omega_o t + \varphi_o + 30°) \\ \cos(\omega_o t + \varphi_o + 30° - 120°) \\ \cos(\omega_o t + \varphi_o + 30° + 120°) \end{bmatrix} \begin{bmatrix} \cos(\omega_i t - \varphi_c - \varphi_i) \\ \cos(\omega_i t - \varphi_c - \varphi_i - 120°) \\ \cos(\omega_i t - \varphi_c - \varphi_i + 120°) \end{bmatrix}^T, \tag{2.21}$$

where m is commonly referred to as modulation index. The output voltage referred to output neutral n, can thus be represented as

$$\mathbf{v_{on}}^{(3)} = \mathbf{m}^{(3)} \mathbf{v_{cf}}^{(3)}, \tag{2.22}$$

where, the input-output phase voltage gain matrix $\mathbf{m}^{(3)}$ is obtained from (2.21) as

$$\mathbf{m}^{(3)} = (m/\sqrt{3}) \begin{bmatrix} \cos(\omega_o t + \varphi_o) \\ \cos(\omega_o t + \varphi_o - 120^\circ) \\ \cos(\omega_o t + \varphi_o + 120^\circ) \end{bmatrix} \begin{bmatrix} \cos(\omega_i t - \varphi_c - \varphi_i) \\ \cos(\omega_i t - \varphi_c - \varphi_i - 120^\circ) \\ \cos(\omega_i t - \varphi_c - \varphi_i + 120^\circ) \end{bmatrix}^T. \tag{2.23}$$

From power balance and gain relationship of (2.22),

$$\mathbf{i_{in}}^{(3)} = \left(\mathbf{m}^{(3)}\right)^T \mathbf{i_o}^{(3)}. \tag{2.24}$$

Instantaneous input-output power balance also implies that

$$\frac{3}{2}\hat{V}_{cf}\hat{I}_{in}\cos\varphi_i = \frac{3}{2}\hat{V}_o\hat{I}_o\cos\varphi_{oL}, \tag{2.25}$$

where, φ_{oL} is the output displacement angle and $\hat{I}_o$ is the amplitude of the output current (i_o). So for a given $\mathbf{v_{on}^*}^{(3)}$, load and $\mathbf{v_{cf}}^{(3)}$, it is not possible to independently control φ_i and $\hat{I}_{in}$. Using (2.25) along with m_v and m_i defined in (2.10) and (2.16) respectively, the modulation index m is evaluated as

$$m \;=\; m_v m_i = \left(\frac{\sqrt{3}\,\hat{V}_o}{V_{dc}}\right)\left(\frac{\hat{I}_{in}}{I_{dc}}\right) = \frac{\sqrt{3}\,\hat{V}_o\hat{I}_{in}}{P_{in}} = \frac{\hat{V}_o}{\frac{\sqrt{3}}{2}\,\hat{V}_{cf}\cos(\varphi_i)}. \tag{2.26}$$

Using (2.25) and (2.26), the magnitude of the input output variables are related as

$$\hat{V}_o = \frac{\sqrt{3}}{2} m\,\hat{V}_{cf}\cos(\varphi_i) \quad \text{and} \quad \hat{I}_{in} = \frac{\sqrt{3}}{2} m\,\hat{I}_o\cos(\varphi_{oL}). \tag{2.27}$$

Now, when both $\bar{\mathbf{V}}_{\mathbf{oL}}^*$ and $\bar{\mathbf{I}}_{\mathbf{in}}^*$ are in sector I of their corresponding hexagons, using (2.11) and (2.18), the input phase to output line voltage low frequency gain matrix is obtained as

$$\mathbf{m_v}\{\mathbf{m_i}\}^T = \begin{bmatrix} d_\alpha + d_\beta \\ -d_\alpha \\ -d_\beta \end{bmatrix} \begin{bmatrix} d_\mu + d_\gamma \\ -d_\mu \\ -d_\gamma \end{bmatrix}^T. \tag{2.28}$$

Therefore the average output line voltages over a switching cycle T_s are

$$\begin{bmatrix} v_{AB} \\ v_{BC} \\ v_{CA} \end{bmatrix} = \begin{bmatrix} d_\alpha + d_\beta \\ -d_\alpha \\ -d_\beta \end{bmatrix} \begin{bmatrix} d_\mu + d_\gamma \\ -d_\mu \\ -d_\gamma \end{bmatrix}^T \begin{bmatrix} v_a \\ v_b \\ v_c \end{bmatrix}$$

$$= \begin{bmatrix} d_\mu(d_\alpha + d_\beta)(v_a - v_b) - d_\gamma(d_\alpha + d_\beta)(v_c - v_a) \\ -d_\alpha d_\mu(v_a - v_b) + d_\alpha d_\gamma(v_c - v_a) \\ -d_\beta d_\mu(v_a - v_b) + d_\beta d_\gamma(v_c - v_a) \end{bmatrix}$$

$$= \begin{bmatrix} d_\mu(d_\alpha + d_\beta) \\ -d_\alpha d_\mu \\ -d_\beta d_\mu \end{bmatrix} v_{ab} + \begin{bmatrix} -d_\gamma(d_\alpha + d_\beta) \\ d_\alpha d_\gamma \\ d_\beta d_\gamma \end{bmatrix} v_{ca}. \tag{2.29}$$

Thus there are four combinations of duty cycles $d_\alpha d_\mu$, $d_\alpha d_\gamma$, $d_\beta d_\mu$ and $d_\beta d_\gamma$ corresponding to the active states $V_\alpha I_\mu$, $V_\alpha I_\gamma$, $V_\beta I_\mu$ and $V_\beta I_\gamma$. Using (2.10), (2.16) and (2.26), the duty cycle for the active state $V_\alpha I_\mu$ is

$$\begin{aligned} d_\alpha d_\mu &= \frac{\sqrt{3}\,\hat{V}_o}{V_{dc}} \frac{\hat{I}_{in}}{I_{dc}} \sin(60^\circ - \theta_{SV}) \sin(60^\circ - \theta_{SI}) \\ &= m \sin(60^\circ - \theta_{SV}) \sin(60^\circ - \theta_{SI}). \end{aligned} \tag{2.30}$$

Similarly, the following are derived

$$\begin{aligned} d_\alpha d_\gamma &= m \sin(60^\circ - \theta_{SV}) \sin(\theta_{SI}), \\ d_\beta d_\mu &= m \sin(\theta_{SV}) \sin(60^\circ - \theta_{SI}), \\ d_\beta d_\gamma &= m \sin(\theta_{SV}) \sin(\theta_{SI}). \end{aligned} \tag{2.31}$$

The input-output connections over a switching period in the decoupled construct and the corresponding connections in the actual matrix topology are shown in Table 2.7.

Table 2.7 Mapping from CSC VSC construct to 9 Qsw MC

	CSC VSC construct					3 Ph MC		
ON time	A	B	C	+	–	A	B	C
$d_\alpha d_\mu T_S$	+	–	+	a	b	a	b	a
$d_\beta d_\mu T_S$	+	–	–	a	b	a	b	b
$d_\alpha d_\gamma T_S$	+	–	+	a	c	a	c	a
$d_\beta d_\gamma T_S$	+	–	–	a	c	a	c	c

2.1.1.1 Transformation of 3 Phase Variables in *abc* Domain to *dq* Domain

In this analysis the modelling of the system has been carried out in a synchronously rotating (dq) domain. The advantage of working in the dq domain are that the fundamental frequency components of all variables which were varying sinusoidally in abc domain are transformed to time invariant quantities in steady state. This greatly simplifies the task of analysis and controller design.

The 3 Ph variables of (2.22) in abc domain are transformed to a synchronously rotating (dq) frame using the transfer matrix

$$\mathbf{T} = \sqrt{\frac{2}{3}} \begin{bmatrix} \cos(\omega_T t) & \cos(\omega_T t - 120^\circ) & \cos(\omega_T t + 120^\circ) \\ \sin(\omega_T t) & \sin(\omega_T t - 120^\circ) & \sin(\omega_T t + 120^\circ) \\ 1/\sqrt{2} & 1/\sqrt{2} & 1/\sqrt{2} \end{bmatrix}, \tag{2.32}$$

in the following manner

$$\mathbf{v_{on}} = \begin{bmatrix} v_{ond} \\ v_{onq} \\ v_{on0} \end{bmatrix} = \mathbf{T}\mathbf{v_{on}}^{(3)} = \left(\mathbf{T}\mathbf{m}^{(3)}\mathbf{T}^{-1}\right)\mathbf{T}\mathbf{v_{cf}}^{(3)} = \mathbf{m} \begin{bmatrix} v_{cfd} \\ v_{cfq} \\ v_{cf0} \end{bmatrix} = \mathbf{m}\,\mathbf{v_{cf}}. \tag{2.33}$$

Here, $\omega_T t$ is estimated by a PLL locked to the phase—a of the point of common coupling (PCC). For synchronous applications, $\omega_T = \omega_o = \omega_i$. Since balanced 3-phase system has been considered, the zero sequence components can be neglected. The output-input voltage relationship in (2.33) gets modified to

$$\mathbf{v_{on}} = \begin{bmatrix} v_{ond} \\ v_{onq} \end{bmatrix} = \mathbf{m}\,\mathbf{v_{cf}} = \mathbf{m} \begin{bmatrix} v_{cfd} \\ v_{cfq} \end{bmatrix}, \tag{2.34}$$

where, the gain matrix $\mathbf{m}$ is obtained using (2.22), (2.23) and (2.32), as

$$\mathbf{m} = \frac{\sqrt{3}}{2} m \begin{bmatrix} \cos\varphi_o \\ \sin\varphi_o \end{bmatrix} \begin{bmatrix} \cos\theta_i & \sin\theta_i \end{bmatrix} = \begin{bmatrix} m_d \\ m_q \end{bmatrix} \begin{bmatrix} \cos\theta_i & \sin\theta_i \end{bmatrix}. \tag{2.35}$$

Here,

$$\theta_i = \varphi_i + \varphi_c. \tag{2.36}$$

m_d and m_q allow complete control on the voltage gain of MC and θ_i on the input displacement angle.

The input currents are obtained as

$$\mathbf{i_{in}} = \mathbf{m}^T \mathbf{i_o}. \tag{2.37}$$

Fig. 2.6 Low frequency gain of MC

This concludes the discussion on the low frequency gain of MC. The 'black box' model of the low frequency gain of MC is shown in Fig. 2.6. Dynamic modelling is discussed in the next section.

2.2 Linearized Model

Figure 2.7 shows the single phase equivalent of the overall system where the source impedance has been modelled as an inductance L_s. **P** represents the PCC. An output ripple filter is also necessary to attenuate the switching frequency components in the voltage waveforms.

Referring to Fig. 2.7, dynamic equations for i_o and v_{cf} in abc domain are,

$$\frac{d}{dt}\mathbf{i_o}^{(3)} = \frac{1}{L_o}\left(\mathbf{v_{on}}^{(3)} - \mathbf{v_{co}}^{(3)}\right) \quad \text{and} \quad \frac{d}{dt}\mathbf{v_{cf}}^{(3)} = \frac{1}{C_f}\left(\mathbf{i_s}^{(3)} - \mathbf{i_{in}}^{(3)}\right). \tag{2.38}$$

Substituting $\mathbf{v_{on}}^{(3)}$ and $\mathbf{i_{in}}^{(3)}$ in (2.38) by applying the gain equations (2.22) and (2.24), leads to

$$\frac{d}{dt}\mathbf{i_o}^{(3)} = \frac{1}{L_o}\left(\mathbf{m}^{(3)}\mathbf{v_{cf}}^{(3)} - \mathbf{v_{co}}^{(3)}\right) \quad \text{and} \quad \frac{d}{dt}\mathbf{v_{cf}}^{(3)} = \frac{1}{C_f}\left(\mathbf{i_s}^{(3)} - \left(\mathbf{m}^{(3)}\right)^T \mathbf{i_o}^{(3)}\right). \tag{2.39}$$

These equations are transformed to dq domain using the transfer matrix **T** in (2.32). Subsequent omission of the zero sequence components in the transformed equations results in

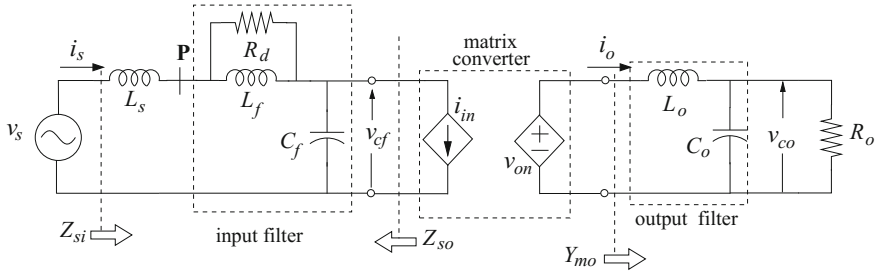

Fig. 2.7 Single phase diagram including source inductance

$$\frac{d}{dt}\mathbf{i}_o = \begin{bmatrix} 0 & -\omega_T \\ \omega_T & 0 \end{bmatrix}\mathbf{i_o} + \frac{1}{L_o}\left(\mathbf{m}\mathbf{v_{cf}} - \mathbf{v_{co}}\right), \tag{2.40}$$

$$\frac{d}{dt}\mathbf{v}_{cf} = \begin{bmatrix} 0 & -\omega_T \\ \omega_T & 0 \end{bmatrix}\mathbf{v_{cf}} + \frac{1}{C_f}\left(\mathbf{i_s} - \mathbf{m}^T\mathbf{i_o}\right). \tag{2.41}$$

Equations (2.40) and (2.41) are nonlinear as product of states ($\mathbf{v_{cf}}$, $\mathbf{i_o}$) and inputs ($\mathbf{m}$) are involved. These are linearized around an equilibrium point (I_{sd}, I_{sq}, I_{Lfd}, I_{Lfq}, V_{cfd}, V_{cfq}, I_{od}, I_{oq}, V_{cod}, V_{coq}, V_{sd} and V_{sq}). Denoting equilibrium value of a variable x as X and a small perturbation in x around X as $\tilde{x}$, the equations corresponding to (2.40) and (2.41) in the linearized model are

$$\frac{d}{dt}\tilde{\mathbf{i}}_o = \begin{bmatrix} 0 & -\omega_T \\ \omega_T & 0 \end{bmatrix}\tilde{\mathbf{i}}_o + \frac{1}{L_o}\left(\tilde{\mathbf{m}}\mathbf{V_{cf}} + \mathbf{M}\,\tilde{\mathbf{v}}_{\mathbf{cf}} - \tilde{\mathbf{v}}_{\mathbf{co}}\right), \tag{2.42}$$

$$\frac{d}{dt}\tilde{\mathbf{v}}_{\mathbf{cf}} = \begin{bmatrix} 0 & -\omega_T \\ \omega_T & 0 \end{bmatrix}\tilde{\mathbf{v}}_{\mathbf{cf}} + \frac{1}{C_f}\left(\tilde{\mathbf{i}}_s - \tilde{\mathbf{m}}^T\mathbf{I_o} - \mathbf{M}^T\tilde{\mathbf{i}}_{\mathbf{o}}\right). \tag{2.43}$$

$\tilde{\mathbf{m}}$ and $\mathbf{M}$ are obtained using (2.35) as,

$$\mathbf{m} = \mathbf{M} + \tilde{\mathbf{m}} = \begin{bmatrix} M_d + \tilde{m}_d \\ M_q + \tilde{m}_q \end{bmatrix}\begin{bmatrix} \cos(\theta_i + \tilde{\theta}_i) \\ \sin(\theta_i + \tilde{\theta}_i) \end{bmatrix}^T$$

$$= \underbrace{\begin{bmatrix} M_d \\ M_q \end{bmatrix}\begin{bmatrix} C_\theta & S_\theta \end{bmatrix}}_{\mathbf{M}} + \underbrace{\begin{bmatrix} \tilde{m}_d \\ \tilde{m}_q \end{bmatrix}\begin{bmatrix} C_\theta & S_\theta \end{bmatrix} + \begin{bmatrix} -M_d S_\theta & M_d C_\theta \\ -M_q S_\theta & M_q C_\theta \end{bmatrix}\tilde{\theta}_i}_{\tilde{\mathbf{m}}} \tag{2.44}$$

where

$$\cos\theta_i = C_\theta \quad \text{and} \quad \sin\theta_i = S_\theta. \tag{2.45}$$

So far, the analysis was carried out in time domain to highlight the source of nonlinearity in the dynamic equations and the consequent requirement of linearizing them. Continuing the system description with dynamic equations in time domain invariably leads to state space description and subsequently eigenvalue analysis using computational tools. It is very difficult to correlate the eigenvalues with the passive components, among which the filter elements are actually design parameters. Consequently, an understanding of how the system dynamics are affected by hardware design and different operating points cannot be developed. Hence, this route has been consciously avoided in this book. Therefore, the system modelling from now onwards will be discussed in s domain which enables use of transfer functions.

Before detailing the 3 Ph small signal model, the transfer functions of interest in the per-phase system of Fig. 2.7 are described. The input filter output impedance, Z_{so} is defined as

$$Z_{so}(s) = -\frac{v_{cf}(s)}{i_{in}(s)}\bigg|_{v_s(s)=0} = \frac{s^2 L_s L_f + R_d(L_s + L_f)s}{s^3 L_s L_f C_f + s^2(L_s + L_f)R_d C_f + sL_f + R_d}. \tag{2.46}$$

Input impedance seen from source, Z_{si} is

$$Z_{si}(s) = \frac{v_s(s)}{i_s(s)}\bigg|_{i_{in}(s)=0} = \frac{s^3 L_s L_f C_f + s^2(L_s + L_f)R_d C_f + sL_f + R_d}{(sL_f + R_d)sC_f}, \tag{2.47}$$

and the output admittance seen from the converter output terminals Y_{mo}, is

$$Y_{mo}(s) = \frac{1}{Z_{mo}(s)} = \frac{i_o(s)}{v_{on}(s)} = \frac{1}{R_o}\frac{1 + sR_oC_o}{s^2 L_o C_o + s\frac{L_o}{R_o} + 1}. \tag{2.48}$$

The forward gain for the input and output filter are

$$G_{fv}(s) = \frac{v_{cf}(s)}{v_s(s)}\bigg|_{i_{in}(s)=0} = \frac{i_s(s)}{i_{in}(s)}\bigg|_{v_s(s)=0} = \frac{1}{sC_f}\frac{1}{Z_{si}(s)}, \tag{2.49}$$

$$G_{vof}(s) = \frac{v_{co}(s)}{v_{on}(s)} = \frac{1}{s^2 L_o C_o + s\frac{L_o}{R_o} + 1}. \tag{2.50}$$

Hence in the per-phase system, $i_s(s)$ can be described as

$$\begin{aligned} i_s(s) &= \frac{i_s(s)}{i_{in}(s)}\bigg|_{v_s=0} i_{in}(s) \quad + \quad \frac{i_s(s)}{v_s(s)}\bigg|_{i_{in}=0} v_s(s) \\ &= G_{fv}(s) i_{in}(s) \quad + \quad Z_{si}^{-1}(s) v_s(s). \end{aligned} \tag{2.51}$$

Therefore in abc domain for a balanced 3 Ph system,

$$\mathbf{i_s}^{(3)}(s) = \mathbf{I_3} G_{fv}(s) \mathbf{i_{in}}^{(3)}(s) \quad + \quad \mathbf{I_3} Z_{si}^{-1}(s) \mathbf{v_s}^{(3)}(s), \tag{2.52}$$

where $\mathbf{I_3}$ represents a 3×3 identity matrix.

Whenever any transfer function matrix for a balanced 3 Ph system $\mathbf{I_3}G(s)$ in abc domain is transformed to dq domain, it results in a non-diagonal (coupled) transfer matrix $\mathbf{G}(s)$ [41]. The transformed matrix $\mathbf{G}(s)$ is represented in the form

$$\mathbf{G}(s) = \begin{bmatrix} G_{11}(s) & G_{12}(s) \\ -G_{12}(s) & G_{11}(s) \end{bmatrix}, \tag{2.53}$$

where the individual elements are

$$G_{11}(s) = \frac{1}{2}\left\{G(s + j\omega_T) + G(s - j\omega_T)\right\},$$
$$G_{12}(s) = -\frac{j}{2}\left\{G(s + j\omega_T) - G(s - j\omega_T)\right\}. \tag{2.54}$$

For example, $\mathbf{I_3}G_{fv}(s)$ is transformed to $\mathbf{G_{fv}}(s)$ as

$$\mathbf{G_{fv}}(s) = \begin{bmatrix} G_{fv11}(s) & G_{fv12}(s) \\ -G_{fv12}(s) & G_{fv11}(s) \end{bmatrix}, \quad \text{where,}$$
$$G_{fv11}(s) = \frac{1}{2}\left\{G_{fv}(s + j\omega_T) + G_{fv}(s - j\omega_T)\right\} \;\&$$
$$G_{fv12}(s) = -\frac{j}{2}\left\{G_{fv}(s + j\omega_T) - G_{fv}(s - j\omega_T)\right\}. \tag{2.55}$$

$\mathbf{Z_{si}^{-1}}(s)$ can be similarly derived from its per phase counterpart $Z_{si}^{-1}(s)$. Hence (2.52) can be described in dq domain as

$$\mathbf{i_s}(s) = \mathbf{G_{fv}}(s)\mathbf{i_{in}}(s) \quad + \quad \mathbf{Z_{si}^{-1}}(s)\mathbf{v_s}(s). \tag{2.56}$$

From (2.56), the perturbed variable $\tilde{\mathbf{i}}_\mathbf{s}(s)$ in the linear model can be described as

$$\tilde{\mathbf{i}}_\mathbf{s}(s) = \mathbf{G_{fv}}(s)\,\tilde{\mathbf{i}}_\mathbf{in}(s) + \mathbf{Z_{si}^{-1}}(s)\tilde{\mathbf{v}}_\mathbf{s}(s). \tag{2.57}$$

Using the transfer matrix notation of (2.53), (2.57) can be expanded as

$$\begin{bmatrix} \tilde{i}_{sd}(s) \\ \tilde{i}_{sq}(s) \end{bmatrix} = \begin{bmatrix} G_{fv11}(s) & G_{fv12}(s) \\ -G_{fv12}(s) & G_{fv11}(s) \end{bmatrix} \begin{bmatrix} \tilde{i}_{ind}(s) \\ \tilde{i}_{inq}(s) \end{bmatrix} + \begin{bmatrix} Z_{si11}^{-1}(s) & Z_{si12}^{-1}(s) \\ -Z_{si12}^{-1}(s) & Z_{si11}^{-1}(s) \end{bmatrix} \begin{bmatrix} \tilde{v}_{sd}(s) \\ \tilde{v}_{sq}(s) \end{bmatrix}. \tag{2.58}$$

Similarly, other perturbed variables in dq domain can be described using the per-phase equations (2.46)–(2.50), as

$$\tilde{\mathbf{v}}_\mathbf{cf}(s) = \mathbf{G_{fv}}(s)\tilde{\mathbf{v}}_\mathbf{s}(s) - \mathbf{Z_{so}}(s)\,\tilde{\mathbf{i}}_\mathbf{in}(s), \tag{2.59}$$
$$\tilde{\mathbf{i}}_\mathbf{o}(s) = \mathbf{Y_{mo}}(s)\,\tilde{\mathbf{v}}_\mathbf{on}(s) = \mathbf{Z_{mo}^{-1}}(s)\,\tilde{\mathbf{v}}_\mathbf{on}(s), \tag{2.60}$$
$$\tilde{\mathbf{v}}_\mathbf{co}(s) = \mathbf{G_{vof}}(s)\,\tilde{\mathbf{v}}_\mathbf{on}(s). \tag{2.61}$$

Using (2.34), (2.37) and (2.44), the gain equations in the linearized model are obtained as

$$\tilde{\mathbf{v}}_\mathbf{on}(s) = \tilde{\mathbf{m}}(s)\mathbf{V_{cf}} + \mathbf{M}\,\tilde{\mathbf{v}}_\mathbf{cf}(s), \tag{2.62}$$
$$\tilde{\mathbf{i}}_\mathbf{in}(s) = (\tilde{\mathbf{m}}(s))^T\,\mathbf{I_o} + \mathbf{M}^T\,\tilde{\mathbf{i}}_\mathbf{o}(s). \tag{2.63}$$

The 3 Ph small signal model in dq domain is completely described by (2.57)–(2.63), the equivalent circuit of which is shown in Fig. 2.8. Figure 2.8a, b represent

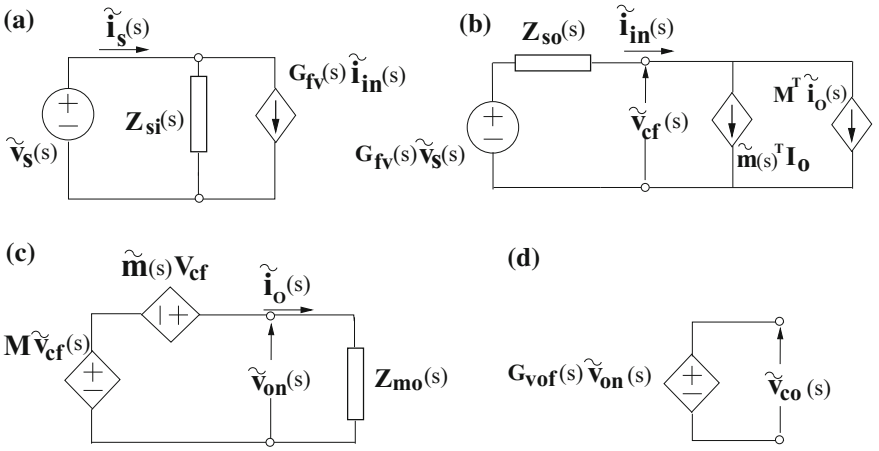

Fig. 2.8 Equivalent circuit of the linearized system. **a**, **b** Input, **c**, **d** Output side

the input side described by (2.57), (2.59) and (2.63). The output side described by (2.60), (2.61) and (2.62) is represented by Fig. 2.8c, d.

The output variables in this model are the voltages $\tilde{\mathbf{v}}_{\mathbf{co}}(s)$ across the output filter capacitors and the q-axis (reactive) component of source current, $\tilde{i}_{sq}(s)$. From (2.44), the control inputs are $\tilde{m}_d(s)$, $\tilde{m}_q(s)$ and $\tilde{\theta}_i(s)$. In the present analysis, the output filter voltages are the only variables which are being controlled. Thus, θ_i is assumed to be set at an arbitrary constant value θ_I, leaving $\left[\tilde{m}_d(s)\ \tilde{m}_q(s)\right]^T$ as the only control inputs while $\tilde{\mathbf{v}}_{\mathbf{co}}(s)(=\left[\tilde{v}_{cod}(s)\ \tilde{v}_{coq}(s)\right]^T)$ are the output variables of the dynamic model. The steps for deriving the input to output transfer matrix are described subsequently, where, the disturbance inputs $\tilde{\mathbf{v}}_{\mathbf{s}}(s)$ are not considered.

Substituting $\tilde{\mathbf{i}}_{\mathbf{in}}(s)$ from (2.63) in (2.59), and dropping the Laplace operator in the notation yields

$$\tilde{\mathbf{v}}_{\mathbf{cf}} = -\mathbf{Z_{so}}\tilde{\mathbf{m}}^T\mathbf{I_o} - \mathbf{Z_{so}}\mathbf{M}^T\,\tilde{\mathbf{i}}_{\mathbf{o}}. \tag{2.64}$$

Subsequent substitution of $\tilde{\mathbf{i}}_{\mathbf{o}}$ from (2.60) in (2.64) results in

$$\tilde{\mathbf{v}}_{\mathbf{cf}} = -\mathbf{Z_{so}}\tilde{\mathbf{m}}^T\mathbf{I_o} - \mathbf{Z_{so}}\mathbf{M}^T\,\mathbf{Y_{mo}}\,\tilde{\mathbf{v}}_{\mathbf{on}}. \tag{2.65}$$

Thereafter substituting $\tilde{\mathbf{v}}_{\mathbf{cf}}$ from (2.65) in (2.62) yields

$$\tilde{\mathbf{v}}_{\mathbf{on}} = \tilde{\mathbf{m}}\mathbf{V_{cf}} - \mathbf{M}\,\mathbf{Z_{so}}\tilde{\mathbf{m}}^T\mathbf{I_o} - \mathbf{M}\,\mathbf{Z_{so}}\mathbf{M}^T\,\mathbf{Y_{mo}}\,\tilde{\mathbf{v}}_{\mathbf{on}}$$

$$\Longrightarrow \left(\mathbf{I_2} + \mathbf{M}\mathbf{Z_{so}}\mathbf{M}^T\mathbf{Y_{mo}}\right)\tilde{\mathbf{v}}_{\mathbf{on}} = \left(\tilde{\mathbf{m}}\mathbf{V_{cf}} - \mathbf{M}\mathbf{Z_{so}}\tilde{\mathbf{m}}^T\mathbf{I_o}\right). \tag{2.66}$$

where $\mathbf{I_2}$ represents a 2×2 identity matrix. Denoting $\mathbf{I_2} + \mathbf{MZ_{so}M}^T\mathbf{Y_{mo}}$ as

$$\mathbf{G_I} = \mathbf{I_2} + \mathbf{MZ_{so}M}^T\mathbf{Y_{mo}}, \tag{2.67}$$

$\tilde{\mathbf{v}}_{\mathbf{on}}$ in (2.66) can be expressed as

$$\tilde{\mathbf{v}}_{\mathbf{on}} = \mathbf{G_I}^{-1}\left(\tilde{\mathbf{m}}\mathbf{V_{cf}} - \mathbf{MZ_{so}}\tilde{\mathbf{m}}^T\mathbf{I_o}\right). \tag{2.68}$$

Expanded form of $\mathbf{G_I}^{-1}$ is derived in (A.3) of Appendix A.1. It has also been shown in Appendix A.2 that $\tilde{\mathbf{m}}\mathbf{V_{cf}} - \mathbf{MZ_{so}}\tilde{\mathbf{m}}^T\mathbf{I_o}$ can be simplified to

$$\left(\tilde{\mathbf{m}}\mathbf{V_{cf}} - \mathbf{MZ_{so}}\tilde{\mathbf{m}}^T\mathbf{I_o}\right) = \mathbf{G_a}(s)\begin{bmatrix}\tilde{m}_d \\ \tilde{m}_q\end{bmatrix}, \tag{2.69}$$

where

$$\mathbf{G_a}(s) = \begin{bmatrix} a_V - M_d Z_{so11} I_{od} & -M_d Z_{so11} I_{oq} \\ -M_q Z_{so11} I_{od} & a_V - M_q Z_{so11} I_{oq}\end{bmatrix} \tag{2.70}$$

and

$$a_V = \sqrt{\frac{3}{2}}\hat{V}_{cf}\cos\varphi_i. \tag{2.71}$$

Therefore using (2.68) and (2.69),

$$\tilde{\mathbf{v}}_{\mathbf{on}} = \mathbf{G_I}^{-1}\mathbf{G_a}\begin{bmatrix}\tilde{m}_d \\ \tilde{m}_q\end{bmatrix}. \tag{2.72}$$

Finally, substituting $\tilde{\mathbf{v}}_{\mathbf{on}}$ from (2.72) in (2.61), the input to output equations after re-introducing the Laplace operator are

$$\tilde{\mathbf{v}}_{\mathbf{co}}(s) = \mathbf{G_{vof}}(s)\tilde{\mathbf{v}}_{\mathbf{on}}(s) = \mathbf{G_{vof}}(s)\mathbf{G_I}^{-1}(s)\mathbf{G_a}(s)\begin{bmatrix}\tilde{m}_d(s) \\ \tilde{m}_q(s)\end{bmatrix} = \mathbf{G_c}(s)\begin{bmatrix}\tilde{m}_d(s) \\ \tilde{m}_q(s)\end{bmatrix}. \tag{2.73}$$

The control plant transfer function matrix $\mathbf{G_c}(s)$ is a function of both input and output filter parameters as well as the operating points. However it is not apparent how these factors affect the poles and zeros of $\mathbf{G_c}(s)$. From the perspective of controller design the question that immediately arises is whether the plant is stable under all operating conditions. Another related concern is the possibility of non-minimum phase zeros appearing in the plant. These are discussed in the following section.

2.3 Composition of $\mathbf{G_c}(s)$

The first objective of the analysis is to examine whether the plant is stable at all operating points i.e. to detect the presence of any right half poles (RHPs) in $\mathbf{G_c}(s)$. This is accomplished by looking into the 3 component matrices of $\mathbf{G_c}(s)$. Also, another objective is to find out whether the plant contains any right half zeros (RHZs).

It has been shown in Appendix A.3, that all the component matrices of $\mathbf{G_c}(s)$ belong to a special category, where all four elements in each of the component matrices have a common denominator polynomial. Therefore all entries in $\mathbf{G_a}(s)$ have a common denominator polynomial and the same holds true for both $\mathbf{G_I}^{-1}(s)$ and $\mathbf{G_{vof}}(s)$. Analysis of poles and zeros for this specific sub class of common denominator transfer function matrices (CdTM) are described in the following section.

2.3.1 Poles and Zeros of CdTM

A 2×2 transfer matrix $\mathbf{G}(s)$ with normal rank 2 is considered where

$$\mathbf{G}(s) = \begin{bmatrix} G_{11}(s) & G_{12}(s) \\ G_{21}(s) & G_{22}(s) \end{bmatrix} = \frac{1}{d(s)} \begin{bmatrix} N_{11}(s) & N_{12}(s) \\ N_{21}(s) & N_{22}(s) \end{bmatrix}. \tag{2.74}$$

$d(s)$ is the common denominator polynomial of each elements and $N_{11}(s)$, $N_{12}(s)$, $N_{21}(s)$ and $N_{22}(s)$ are the numerator polynomials. The common denominator $d(s)$ and the matrix composed of numerator polynomials will be denoted here as

$$C_d\,(\mathbf{G}) = d(s) \quad \text{and} \quad \mathbf{N}\,(\mathbf{G}) = \begin{bmatrix} N_{11}(s) & N_{12}(s) \\ N_{21}(s) & N_{22}(s) \end{bmatrix}.s \tag{2.75}$$

Identifying the poles and zeros of the 2×2 matrix $\mathbf{G}(s)$, requires deriving a diagonal matrix $\mathbf{L}(s)$ from $\mathbf{G}(s)$ as [42, 43],

$$\mathbf{L}(s) = \mathbf{U1}(s)\mathbf{G}(s)\mathbf{U2}(s). \tag{2.76}$$

Here $\mathbf{U1}(s)$ and $\mathbf{U2}(s)$ are the pre and post multiplication matrices used to transform $\mathbf{G}(s)$ to the diagonal matrix $\mathbf{L}(s)$. Therefore determinant of both $\mathbf{U1}(s)$ and $\mathbf{U2}(s)$ are constant. $\mathbf{L}(s)$ is obtained as

$$\mathbf{L}(s) = \begin{bmatrix} \dfrac{a_1(s)}{b_1(s)} & 0 \\ 0 & \dfrac{a_2(s)}{b_2(s)} \end{bmatrix}, \tag{2.77}$$

where $a_1(s)$, $b_2(s)$ are factors of $a_2(s)$ and $b_1(s)$ respectively. Then the poles and zeros of $\mathbf{G}(s)$ are obtained as the roots of the following equations

$$p(s) = b_1(s)b_2(s) = 0 \quad \& \quad z(s) = a_1(s)a_2(s) = 0. \tag{2.78}$$

So at any frequency, if control on any single output is lost, it indicates that a zero of the multivariable system resides at that particular frequency.

An alternative procedure for finding the poles and zeros is [42, 44]

- pole polynomial is the least common denominator of all non-zero minors of all orders of $\mathbf{G}(s)$.
- zero polynomial is the greatest common divisor of the minor of order 2 i.e. the determinant of $\mathbf{G}(s)$, where the determinant has been adjusted to have the pole polynomial as the denominator.

Without using computational softwares, finding all the pole and zeros, adhering to the described procedures, is a difficult exercise if the order of the polynomials are high. This difficulty becomes greater if the transfer function matrix is composed of several component matrices as in $\mathbf{G_c}(s)$. For the purpose of controller design, it is important to correctly identify non-minimum phase poles and zeros, if there are any. As would be seen in a later chapter, this knowledge is sufficient for designing a controller.

In (2.77), $\mathbf{L}(s)$ is obtained by applying standard matrix row/column operations on $\mathbf{G}(s)$ and therefore determinant of each is a constant multiple of other. Therefore the determinant of $\mathbf{G}(s)$ will be probed, where,

$$det\left(\mathbf{G}(s)\right) = \frac{1}{d^2(s)}\{N_{11}(s)N_{22}(s) - N_{12}(s)N_{21}(s)\} = \frac{1}{C_d^2\left(\mathbf{G}\right)} det\left(\mathbf{N}\left(\mathbf{G}\right)\right). \tag{2.79}$$

There may be some common factors between $C_d^2\left(\mathbf{G}\right)$ and $det\left(\mathbf{N}\left(\mathbf{G}\right)\right)$ in (2.79), which remains in addition to roots of $p(s)$ and $z(s)$. Hence, it cannot be said that $C_d^2\left(\mathbf{G}\right)$ has the same factors as $p(s)$ described in (2.78) or whether it is the least common denominator of all non-zero minors of all orders of $\mathbf{G}(s)$. However at the same time, it can definitely be said that the $p(s)$ is a factor of $C_d^2\left(\mathbf{G}\right)$. Similarly, $z(s)$ is a factor of $det\left(\mathbf{N}\left(\mathbf{G}\right)\right)$. Hence for detecting non-minimum phase poles and zeros of $\mathbf{G}(s)$, it is sufficient to investigate the roots of

$$C_d\left(\mathbf{G}\right) = 0 \quad \text{and} \quad det\left(\mathbf{N}\left(\mathbf{G}\right)\right) = 0. \tag{2.80}$$

2.3.2 Poles and Zeros of $G_c(s)$

On basis of the conclusions of the last section, $\mathbf{G_c}(s)$, which can be represented using (2.73) as,

$$\mathbf{G_c}(s) = \frac{1}{C_d\left(\mathbf{G_{vof}}\right)}\mathbf{N}\left(\mathbf{G_{vof}}\right) \times \frac{1}{C_d\left(\mathbf{G_I^{-1}}\right)}\mathbf{N}\left(\mathbf{G_I^{-1}}\right) \times \frac{1}{C_d\left(\mathbf{G_a}\right)}\mathbf{N}\left(\mathbf{G_a}\right), \tag{2.81}$$

roots of the following needs to be investigated

$$\begin{aligned} C_d\left(\mathbf{G_{vof}}\right) = 0 \quad \text{and} \quad det\left(\mathbf{N}\left(\mathbf{G_{vof}}\right)\right) = 0, \\ C_d\left(\mathbf{G_I}^{-1}\right) = 0 \quad \text{and} \quad det\left(\mathbf{N}\left(\mathbf{G_I}^{-1}\right)\right) = 0, \\ C_d\left(\mathbf{G_a}\right) = 0 \quad \text{and} \quad det\left(\mathbf{N}\left(\mathbf{G_a}\right)\right) = 0. \end{aligned} \tag{2.82}$$

All the per-phase transfer functions defined in (2.46)–(2.50), can be represented in the form

$$D(s) = \frac{D_Z(s)}{D_P(s)}, \tag{2.83}$$

where $D_Z(s)$ and $D_P(s)$ are the numerator and denominator polynomials respectively. Using (2.53) and (2.54), the individual elements of the corresponding transfer matrix $\mathbf{D}(s)$ in dq domain are

$$\begin{aligned} D_{11}(s) &= \frac{1}{2}\left\{\frac{D_Z(s+j\omega_T)}{D_P(s+j\omega_T)} + \frac{D_Z(s-j\omega_T)}{D_P(s-j\omega_T)}\right\}, \\ D_{12}(s) &= -\frac{j}{2}\left\{\frac{D_Z(s+j\omega_T)}{D_P(s+j\omega_T)} - \frac{D_Z(s-j\omega_T)}{D_P(s-j\omega_T)}\right\}. \end{aligned} \tag{2.84}$$

Therefore the common denominator polynomial is

$$C_d\left(\mathbf{D}\right) = D_P(s+j\omega_T)\, D_P(s-j\omega_T). \tag{2.85}$$

The roots of common denominator $C_d\left(\mathbf{D}\right)$ of the transfer matrices are obtained by shifting only the imaginary part of the roots of $D_P(s)$. Therefore the real part of the roots remain unaffected as shown in Fig. 2.9. Hence, if $D(s)$ does not have any RHP, then all the roots of $C_d\left(\mathbf{D}\right)$ lie in the left half and consequently $\mathbf{D}(s)$ cannot have a RHP. So a stable transfer function remains stable after the abc to dq transformation.

Again, determinant of $\mathbf{N}\left(\mathbf{D}\right)$ is

$$\begin{aligned} det\left(\mathbf{N}\left(\mathbf{D}\right)\right) = {} & D_Z(s+j\omega_T)D_P(s-j\omega_T) \\ & \times D_Z(s-j\omega_T)D_P(s+j\omega_T). \end{aligned} \tag{2.86}$$

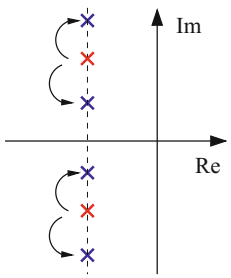

Fig. 2.9 Roots of $D(s)$ and $C_d\left(\mathbf{D}\right)$

So, if $D(s)$ do not have any RHP or RHZ, then det $(\mathbf{N})$ cannot have any root with positive real part either and hence $\mathbf{D}(s)$ cannot have a RHZ. Therefore, since $Z_{so}(s)$, $G_{vof}(s)$ and $Y_{mo}(s)$ do not have any RHP or RHZ, the corresponding transfer matrices in dq domain i.e. $\mathbf{Z_{so}}(s)$, $\mathbf{G_{vof}}(s)$ and $\mathbf{Y_{mo}}(s)$ do not contain any RHP/RHZ either. Therefore C_d $(\mathbf{Z_{so}})$, C_d $(\mathbf{Y_{mo}})$ and C_d $(\mathbf{G_{vof}})$ do not have any root in the right half of s plane.

Now the poles and zeros of the two component matrices $\mathbf{G_I^{-1}}(s)$ and $\mathbf{G_a}(s)$ will be examined.

2.3.2.1 Poles of $\mathbf{G_I^{-1}}(s)$ and $\mathbf{G_a}(s)$

Expression for the common denominator of $\mathbf{G_I^{-1}}(s)$ has been derived in (A.18) as

$$C_d\left(\mathbf{G_I^{-1}}(s)\right) = C_d\left(\mathbf{Y_{mo}}(s)\right) C_d\left(\mathbf{Z_{so}}(s)\right) \left(1 + \underbrace{\frac{3}{4}m^2 Y_{mo11}(s) Z_{so11}(s)}_{G2}\right). \quad (2.87)$$

$C_d\left(\mathbf{Y_{mo}}(s)\right) C_d\left(\mathbf{Z_{so}}(s)\right)$ do not have any root with positive real part. To reduce losses, all input filters are designed to be under damped. Consequently, $Z_{so}(s)$ in (2.46) can be represented with reasonably high accuracy for all frequencies as

$$Z_{so}(s) = \frac{s(L_s + L_f)}{s^2(L_s + L_f)C_f + s\dfrac{L_f^2}{R_d(L_s + L_f)} + 1}. \quad (2.88)$$

In terms of corner frequency (ω_c) and quality factor (Q), $Z_{so}(j\omega)$ can be represented as

$$Z_{so}(j\omega) = \left(L_s + L_f\right) \frac{j\omega}{\left(1 - \dfrac{\omega^2}{\omega_c^2}\right) + j\dfrac{\omega}{Q\omega_c}}, \quad (2.89)$$

where

$$\omega_c \approx \frac{1}{\sqrt{(n+1)L_f C_f}},\ Q \approx Rd\left(\sqrt{\frac{C_f}{L_s}}\right)(1+n)^{1.5}\ \&\ n = \frac{L_s}{L_f}. \quad (2.90)$$

Denoting the following

$$r_\omega = \frac{\omega}{\omega_c} \quad \& \quad K = L_s + L_f, \quad (2.91)$$

$Z_{so}(j\omega)$ in (2.89) can be expressed as

$$Z_{so}(j\omega) = K\omega_c \frac{jr_\omega}{\left(1-r_\omega^2\right)+j\frac{r_\omega}{Q}} = K\omega_c \frac{jr_\omega\left\{\left(1-r_\omega^2\right)-j\frac{r_\omega}{Q}\right\}}{\left(1-r_\omega^2\right)^2+\frac{r_\omega^2}{Q^2}}$$
$$= \quad Pj\left\{\left(1-r_\omega^2\right)-j\frac{r_\omega}{Q}\right\} = P\left\{\frac{r_\omega}{Q}+j\left(1-r_\omega^2\right)\right\}, \tag{2.92}$$

where P is a positive number. Therefore

$$\Re\{Z_{so}(j\omega)\} > 0 \quad \forall\,\omega. \tag{2.93}$$

At the output side for any kind of load, virtual damping can be introduced which would be discussed in a later chapter. So the quality factor of the output filter can be controlled. Consequently, for any kind of load, it can be shown in a very similar manner as done for $Z_{so}(j\omega)$ that

$$\Re\{Y_{mo}(j\omega)\} \geq 0 \quad \forall\,\omega. \tag{2.94}$$

Therefore, using (2.84)

$$\Re\{Z_{so11}(j\omega)\} > 0 \quad \text{and} \quad \Re\{Y_{mo11}(j\omega)\} \geq 0. \tag{2.95}$$

Hence denoting the phase of both $Z_{so11}(j\omega)$ and $Y_{so11}(j\omega)$ as $\angle Z_{so11}(j\omega)$ and $\angle Y_{mo11}(j\omega)$ respectively, the following can be stated

$$-90^\circ < \angle Z_{so11}(j\omega) < 90^\circ \quad \& \quad -90^\circ \leq \angle Y_{mo11}(j\omega) \leq 90^\circ, \tag{2.96}$$

and therefore,

$$-180^\circ < \angle Z_{so11}(j\omega) Y_{mo11}(j\omega) < 180^\circ. \tag{2.97}$$

Hence, plot of $Y_{mo11}(j\omega)Z_{so11}(j\omega)$, for all possible values of filter parameters and load, never encircles the $(-1 + j0)$ point as shown in Fig. 2.10. Therefore from

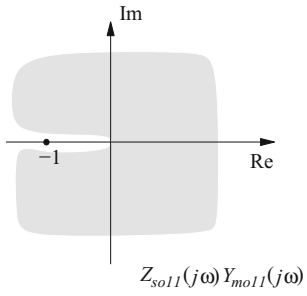

Fig. 2.10 Shaded area encompassing all possible plots of $Y_{mo11}(j\omega)Z_{so11}(j\omega)$

Nyquist criterion it can be concluded that in (2.87), $(1 + G2)$ does not have a root with positive real part. Therefore $\mathbf{G_I}^{-1}(s)$ does not contain a RHP.

$\mathbf{G_a}(s)$ cannot have a RHP either, as from Appendix A.3, its common denominator is

$$C_d\left(\mathbf{G_a}(s)\right) = C_d\left(\mathbf{Z_{so}}(s)\right). \tag{2.98}$$

Since $\mathbf{G_I}^{-1}(s)$, $\mathbf{G_{vof}}(s)$ and $\mathbf{G_a}(s)$ do not contain any RHP, it is therefore concluded that $\mathbf{G_c}(s)$ cannot have any RHP.

2.3.2.2 Zeros of $\mathbf{G_I^{-1}}(s)$ and $\mathbf{G_a}(s)$

Recalling that

$$\mathbf{G_c}(s) = \mathbf{G_{vof}}(s)\mathbf{G_I}^{-1}(s)\mathbf{G_a}(s), \tag{2.99}$$

determinant of $\mathbf{N}\left(\mathbf{G_I}^{-1}(s)\right)$ has been derived in Appendix A.3 as

$$det\left(\mathbf{N}\left(\mathbf{G_I}^{-1}(s)\right)\right) = C_d\left(\mathbf{G_I}^{-1}(s)\right) C_d\left(\mathbf{Y_{mo}}(s)\right) C_d\left(\mathbf{Z_{so}}(s)\right). \tag{2.100}$$

It has been discussed in the last section that $C_d\left(\mathbf{G_I}^{-1}(s)\right)$ does not contain any right half zeros and neither does $C_d\left(\mathbf{Y_{mo}}(s)\right)$ nor $C_d\left(\mathbf{Z_{so}}(s)\right)$. Hence, $\mathbf{G_I}^{-1}(s)$ can not have any RHZ.

So, now focusing on the zeros of $\mathbf{G_a}(s)$, from (A.21)

$$det\left(\mathbf{N}\left(\mathbf{G_a}(s)\right)\right) = C_d^2\left(\mathbf{Z_{so}}(s)\right) a_V^2 \left[1 - \frac{M_d I_{od} + M_q I_{oq}}{a_V} Z_{so11}(s)\right], \tag{2.101}$$

where,

$$\begin{bmatrix} I_{od} \\ I_{oq} \end{bmatrix} = \sqrt{\frac{3}{2}}\,\hat{I}_o \begin{bmatrix} \cos(\varphi_o + \varphi_{oL}) \\ \sin(\varphi_o + \varphi_{oL}) \end{bmatrix}. \tag{2.102}$$

Using (2.27), (2.35), (2.44) and (2.102)

$$M_d I_{od} + M_q I_{oq} = \sqrt{\tfrac{3}{2}}\,\hat{I}_{in}. \tag{2.103}$$

Substituting (2.103) in (2.101),

$$det\left(\mathbf{N}\left(\mathbf{G_a}(s)\right)\right) = C_d^2\left(\mathbf{Z_{so}}(s)\right) a_V^2 \left[1 - \frac{\sqrt{\frac{3}{2}}\hat{I}_{in}}{a_V} Z_{so11}(s)\right]. \tag{2.104}$$

Thereafter using (2.25) along with (2.71) in (2.104),

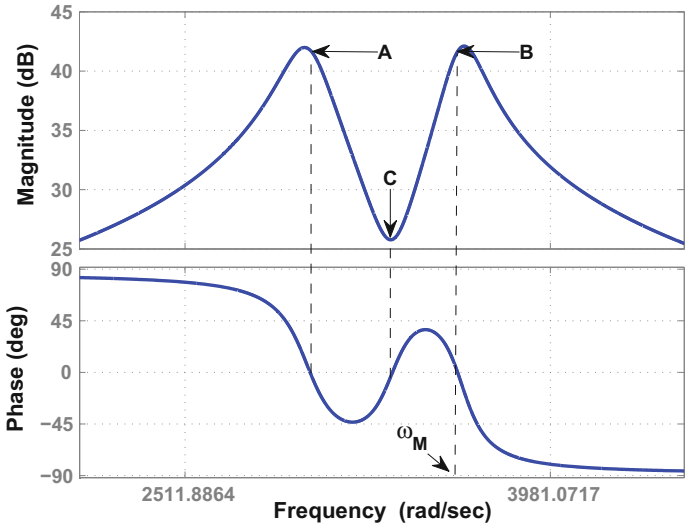

Fig. 2.11 Frequency response of $Z_{so11}(s)$

$$\begin{aligned} det\left(\mathbf{N}\left(\mathbf{G_a}(s)\right)\right) &= C_d^2\left(\mathbf{Z_{so}}(s)\right) a_V^2 \left[1 - \frac{P_{in}}{\frac{3}{2}\hat{V}_{cf}^2 \cos^2\varphi_i} Z_{so11}(s)\right] \\ &= C_d^2\left(\mathbf{Z_{so}}(s)\right) a_V^2 \left[1 - \frac{1}{R_n} Z_{so11}(s)\right]. \end{aligned} \tag{2.105}$$

Frequency response of $Z_{so11}(s)$ is shown in Fig. 2.11. The magnitude plot shows two adjacent peaks near the input filter corner frequency. Also, multiple zero crossing of phase plot is observed. The frequency of the zero phase corresponding to the maximum magnitude is chosen. For a given set of parameters, let point B be that maximum, as shown in Fig. 2.11, corresponding to frequency ω_M. Owing to the presence of negative sign preceding $(1/R_n)\, Z_{so11}$ in (2.105), sufficient condition for avoiding RHZ in $\mathbf{G_a}$, from Nyquist criterion, is

$$\frac{P_{in}}{\frac{3}{2}\hat{V}_{cf}^2 \cos^2\varphi_i} |Z_{so11}(j\omega_M)| < 1, \quad \text{or} \quad P_{in} < \frac{\frac{3}{2}\hat{V}_{cf}^2 \cos^2\varphi_i}{|Z_{so11}(j\omega_M)|} = P_{cr}. \tag{2.106}$$

So, emergence of RHZ depends on the magnitude of voltage at the input terminals, input power factor, power transfer, input filter parameters and source inductance. Moreover, $||Z_{so11}(j\omega)||_\infty$ increases with L_s/L_f ratio and so does $|Z_{so11}(j\omega_M)|$. Hence a higher L_s brings down the P_{in} limit (P_{cr}) for RHZ.

It is noted that the present modelling is achieved without considering the parasitic resistances of the filter elements which increase the overall damping in an actual

plant. Hence, strictly following (2.106) would lead to conservative design. In this context, the parasitic resistances for the inductors depends on the construction, wire gauge etc. which makes it very difficult to address all these aspects in a generic model.

Nevertheless, this analysis gives the system designer an insight into the plant model and a rule to approach the design in an integrated manner. There are two choices—either working with a minimum phase system by appropriate input filter design or designing a suitable controller for a non-minimum phase plant. The former choice simplifies the controller design. However if the load requirement makes the later situation inevitable, then, a proper controller design ensuring stable closed loop operation becomes imperative.

2.4 Concluding Remarks

A model of a grid connected 3ϕ MC has been derived incorporating input, output filters and source inductance. It has been clearly shown that based on a given operating point, RHZs may appear in the control to output transfer function which depends upon the input filter parameters. The power stage of MC along with the presence of input filter is responsible for the emergence of these RHZs in the linearized model. This is clarified with the following example of a generic DC-DC converter having a power stage equivalent to MC.

Example: Figure 2.12 shows the a DC-DC converter where the control objective is to regulate i_o. The input and output voltages and currents are related as

$$v_{on} = d v_{cf} \quad \& \quad i_{in} = d i_o = \frac{d^2 v_{cf}}{R} \tag{2.107}$$

where d, the duty cycle is the control input. The dynamic equation of the state v_{cf} is

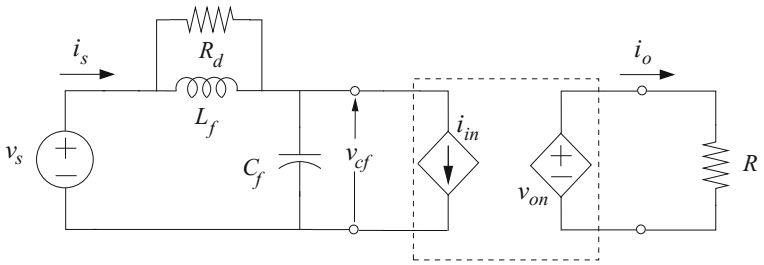

Fig. 2.12 Generic DC-DC converter having same power stage as MC

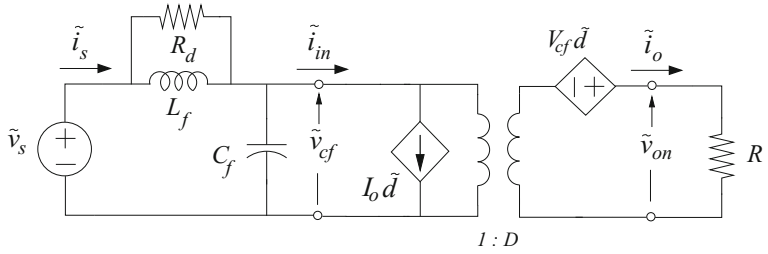

Fig. 2.13 Equivalent circuit of the linearized system

$$\frac{dv_{cf}}{dt} = \frac{1}{C_f}\left(i_s - \frac{d^2 v_{cf}}{R}\right). \tag{2.108}$$

Due to product of the state and control input in (2.108), linearization becomes necessary. In the linearized model shown in Fig. 2.13, the control transfer function is obtained as

$$\frac{\tilde{i}_o(s)}{\tilde{d}(s)} = \frac{V_{cf}}{R}\frac{s^2 L_f C_f + sL_f\left(\frac{1}{R_d} - \frac{D^2}{R}\right) + 1}{s^2 L_f C_f + sL_f\left(\frac{1}{R_d} + \frac{D^2}{R}\right) + 1}. \tag{2.109}$$

Hence RHZs emerge if,

$$\frac{R}{D^2} < R_d, \tag{2.110}$$

i.e. when the load resistance referred to source side is less than the damping resistor. Again since,

$$\frac{R}{D^2} = \frac{V_{on}}{I_o D^2} = \frac{V_{cf}}{I_{in}} = \frac{V_{cf}^2}{P_{in}}, \tag{2.111}$$

therefore, the condition for RHZs described in (2.110), can also be represented as

$$\frac{P_{in}}{V_{cf}^2} > \frac{1}{R_d}. \tag{2.112}$$

Meeting the control requirement i.e. regulation of i_o leads to the origin of the RHZ. From the small signal model, the input side and the output side variables are related as

$$\tilde{v}_{on}(s) = D\tilde{v}_{cf}(s) + V_{cf}\tilde{d}(s),$$
$$\tilde{i}_{in}(s) = D\tilde{i}_{o}(s) + I_{o}\tilde{d}(s). \tag{2.113}$$

Tightly regulated i_o means that irrespective of the variation in v_s, the power transferred to the load P_{in} remains constant. In other words, perfect control demands the following

$$\tilde{v}_{on}(s) = 0, \ \tilde{i}_{o}(s) = 0. \tag{2.114}$$

Using (2.113) and (2.114) results in the following

$$\frac{\tilde{v}_{cf}(s)}{\tilde{i}_{in}(s)} = -\frac{V_{cf}}{DI_o} = -\frac{V_{cf}}{I_{in}} = -\frac{R}{D^2} \tag{2.115}$$

Therefore, under the assumption of perfect regulation the load appears as a negative resistance in the linear model. Any increment in $\tilde{v}_{cf}$ is met with a simultaneous decrement in $\tilde{i}_{in}$, thus exhibiting the typical RHZ characteristics.

The presented analysis is applicable to any other modulation or modelling technique. Thus a design constraint for overall system design has been established which will be used in subsequent chapters where filter and controller design has been detailed.

http://www.springer.com/978-981-10-3829-7

Design and Control of Matrix Converters
Regulated 3-Phase Power Supply and Voltage Sag Mitigation for Linear Loads
Dasgupta, A.; Sensarma, P.
2017, XVI, 124 p. 75 illus., Hardcover
ISBN: 978-981-10-3829-7